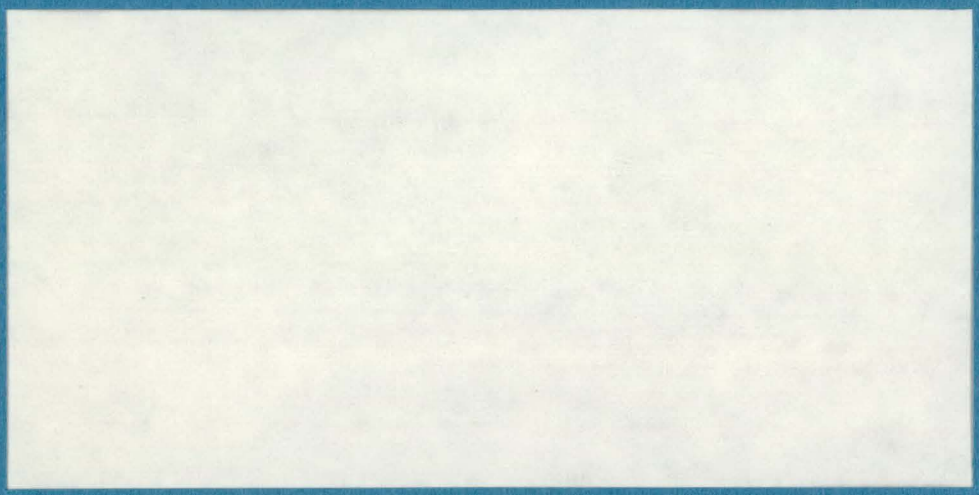

Institute of Energy Conversion

University of Delaware
Newark, Delaware 19711

DISCLAIMER

SERI/PR--9195-1-T3

SERI/PR--9195-1-T3

DE82 006886

"IMPROVED AMORPHOUS Si SOLAR CELLS"

Quarterly Progress Report #5

Contract SERI XG-0-9195-1

February 1, 1981 - April 30, 1981

Supported by Solar Energy Research Institute

November 1981

Institute of Energy Conversion
University of Delaware
Newark, Delaware 19711

"Improved Amorphous Si Solar Cells"

Progress Report

to

Solar Energy Research Institute

Contract: SERI - XG-0-9195-1 Q-5

Period: 1 February 1981 - 30 April 1981

Principal Investigator: Vikram Dalal

Organization: University of Delaware
Institute of Energy Conversion
Newark, Delaware 19711

Date of Report: August 20, 1981

Personnel

The following people contributed to the work reported here:

1. University of Delaware

   Dr. Vikram Dalal, PI

   Dr. Paul Nielsen

   Dr. Fernando Alvarez

   Dr. Erten Eser

   Mr. John Cambridge

   Mr. Kenneth Schubert

   Mr. Timothy Frey

   Mr. Andre Mastrovito

2. University of Chicago

   Professor Helmutt Fritzsche, PI

   Dr. Eric Schiff

   Mr. Peter Persans

Table of Contents

Summary

1. Material Growth

Both n and p-type a-Si:H films with very high conductivities [$\sigma > 10$ (have been grown by diluting SiH_4 in Ar or H_2. These films have Fermi levels close to the conduction and valence bands (~ 0.03 eV). The use these heavily doped films as p^+ and n^+ junction layers in a p^+in^+ cel should increase the diffusion voltage of the diode, thereby increasi both J_{SC} and V_{OC}.

2. Material Analysis

The analysis of conductivity and thermoelectric power on films of dif thickness have revealed no systematic changes. However, the drift mo shows a systematic increase with thickness. We do not yet understand these results.

3. Device Fabrication and Analysis

The analysis of cells by studying QE vs. applied voltage has revealed the electron ($\mu\tau$) product is limiting transport in nip cells and not ($\mu\tau$) product. Analysis reveals that typically $(\mu\tau)_n \approx 10^{-9}$ cm^2/V.

4. Device Design

A new device design, Tandem parallel-connected cells, has been evolved to improve the current collection in a-Si cells. This design may help increase J_{SC} to 15-16 mA/cm^2 in a-Si:H.

I. Material Deposition

The growth of heavily doped, high conductivity n^+ and p^+ layers is a prerequisite for improving the efficiency of a-Si solar cells. The use of high conductivity layers confers several advantages.

1) Reduction in contact resistance.

2) Increase in diffusion voltage. A high conductivity layer with the Fermi level close to the conduction or valence band, allows significant increase in diffusion voltage, which is given by $Eg - E_{f,n} - \Delta E_{f,p}$, where Eg is the bandgap and $\Delta E_{f,n}$, $\Delta E_{f,p}$ are the separation between the Fermi level and the conduction and valence band respectively on the n and p sides of a pin cell. With standard doped layers, $\Delta E_{f,n} \approx 0.15$ - 0.25 eV, and $\Delta E_{f,p} \approx 0.3$ - 0.4 eV. Consequently, the diffusion voltage V_D is only ~ 1.0 - 1.2 V. If $\Delta E_{f,n}$ and $\Delta E_{f,p}$ can be reduced to ~ 0.05 eV, V_D would increase to ~ 1.6 V. This increase in V_D would have two potentially beneficial effects on solar cell performance.

   i) Increased V_D would lead to increased V_{oc}.

   ii) Increased V_D would lead to increased electric field in the i layer, and hence, higher collection efficiency.

Consequently, during this quarter, we have initiated growth of heavily conducting doped a-Si:H films.[1,2].

1) n^+ films. High σ n^+ films were grown from SiH_4:H_2 and SiH_4:Ar mixtures. Typically, SiH_4 was < 5% of total gas content. PH_3 diluted in Ar was used as the dopant gas. Films were grown by RF plasma deposition. A typical $\sigma(T)$ curve is shown in Figure 1. The room-temperature conductivity is $\sigma \approx 20\ (\Omega\text{-cm})^{-1}$. The activation energy is 0.032 eV. The deposition conditions are listed on the figure.

2) p^+ films. High σ p^+ films were difficult to grow by RF deposition. However, DC (cathodic) films readily yielded high conductivity films with heavily diluted SiH_4:H_2 mixtures.[3] However, dilution with Ar did not yield high σ, unlike the case for n^+ films, where Ar seems to help in achieving high .

A typical $\sigma(T)$ curve for high σ p^+ a-Si:H film is shown in Figure 2. The room temperature conductivity is 13 $(\Omega\text{-cm})^{-1}$, and the activation energy is 0.031 eV. Thermoelectric power measurements indicate a p-type layer.

Thus, we have succeeded in growing both n^+ and p^+ high σ layers. These layers are probably microcrystalline,[1] but we have not yet probed the structure of these films.

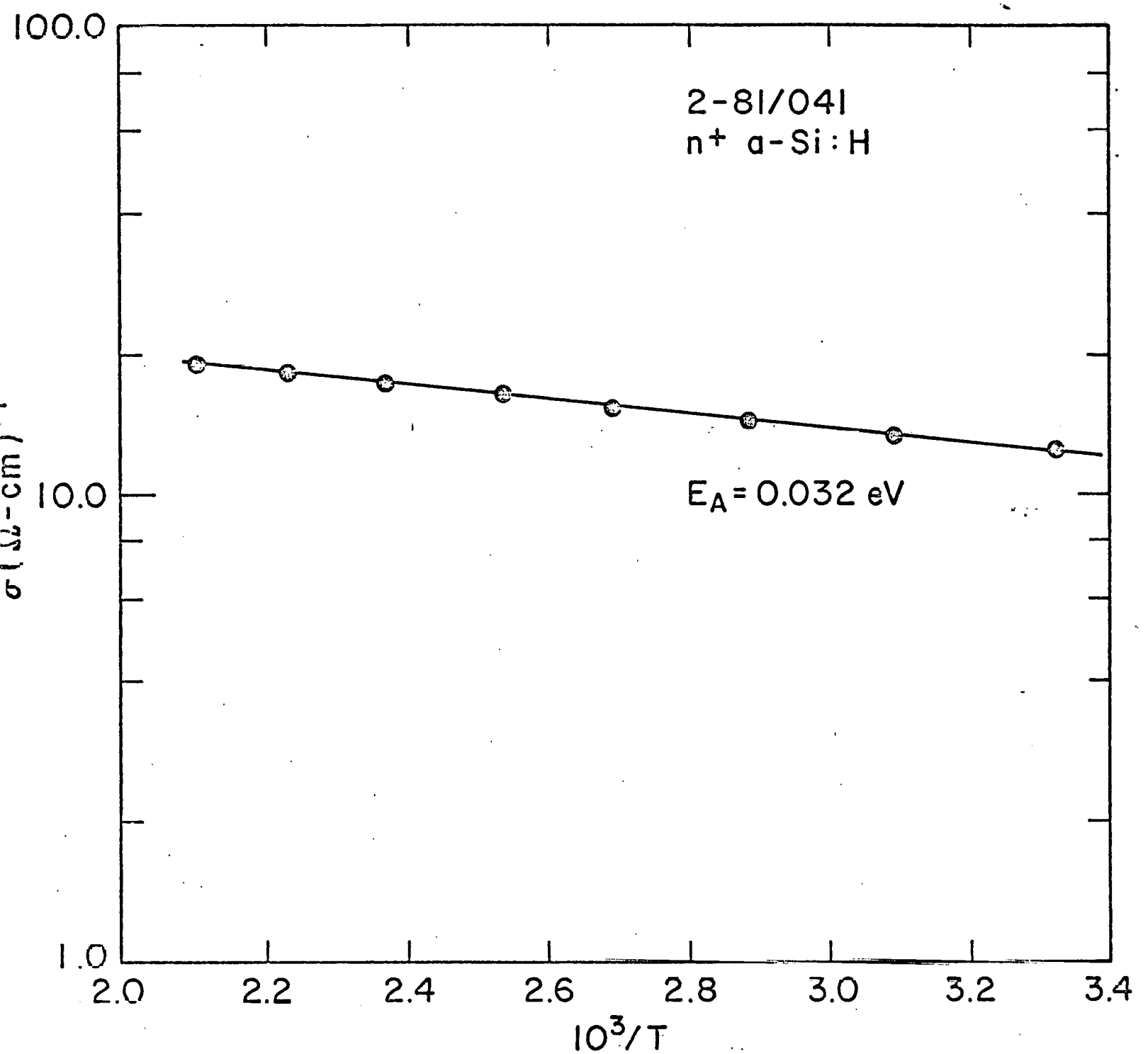

Figure 1. Conductivity of n^+ a-Si:H Doped with p

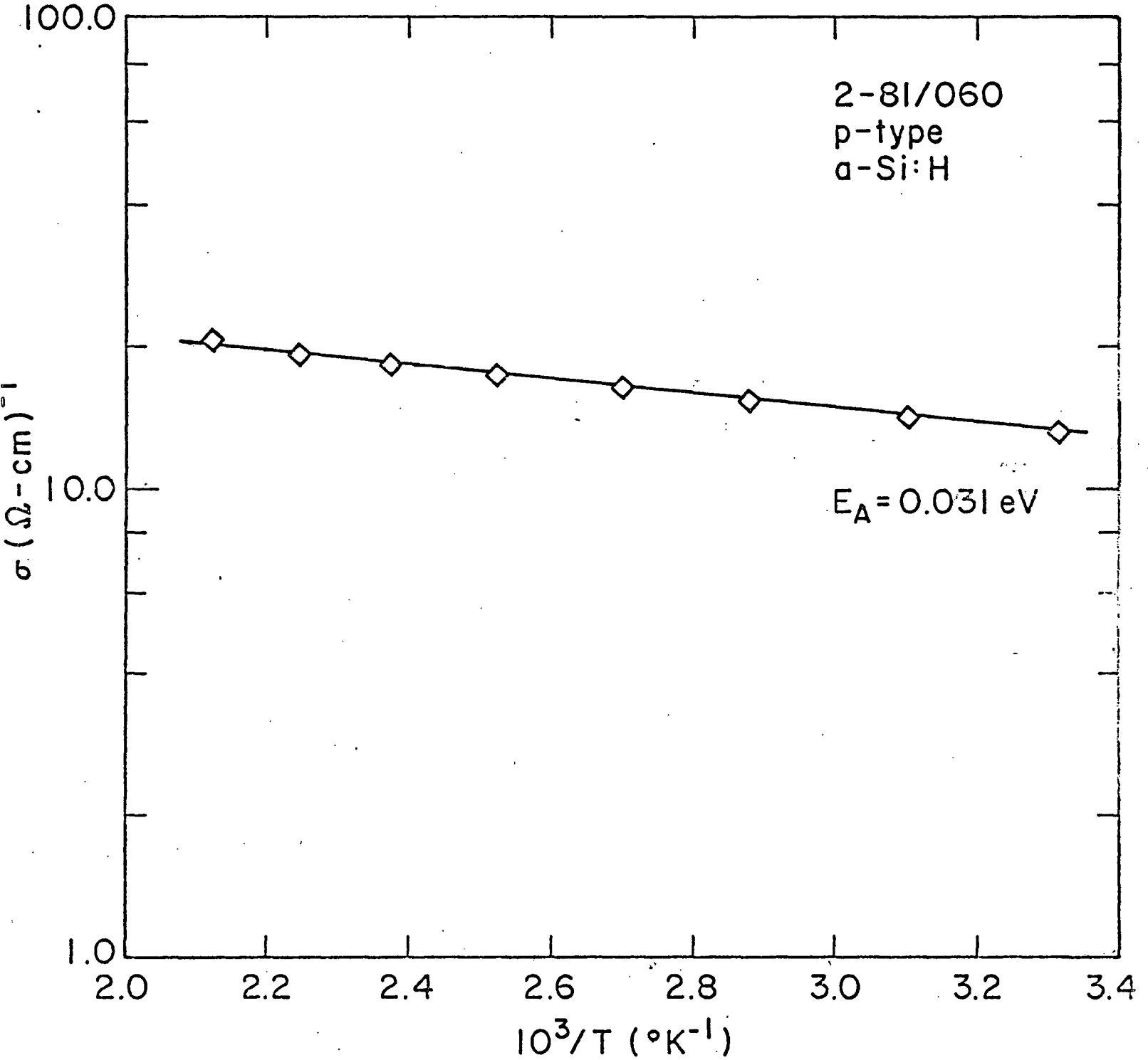

Figure 2. Conductivity of p^+ a-Si:H

II. Material Properties

1. Analysis of Thermoelectric Power in a-Si

A numerical simulation program to study the approximation used by Dohler[4] was developed. It was shown that Dohler's technique works well for predicting Fermi level shift with temperature, but is not as accurate in determining the shape of conductivity-energy relationship. Details of this simulation are in Appendix A.

2. Study of Drift Mobility and σ(T) with Thickness

It was shown previously[5] that electron drift mobility increases with thickness of the sample. To study if this increase in mobility is due to changes in impurity concentration, we studied σ(T), S(T) and mobility on samples prepared at the same time. To do this, films were grown on 7059 slides half-coated with Mo. The half sample on 7059 was used for σ(T) and S(T) studies by methods previously described[6], and the half sample on Mo//059 was used for mobility measurements using the laser time-of-flight technique previously described.

The results are shown in Figure 3, where we plot σ(T) for two different thicknesses. It is seen that there is no significant difference in Fermi level positions (activation energies) between the two films, and yet, the mobilities are very different for the films, with the thicker film having higher μ_n.

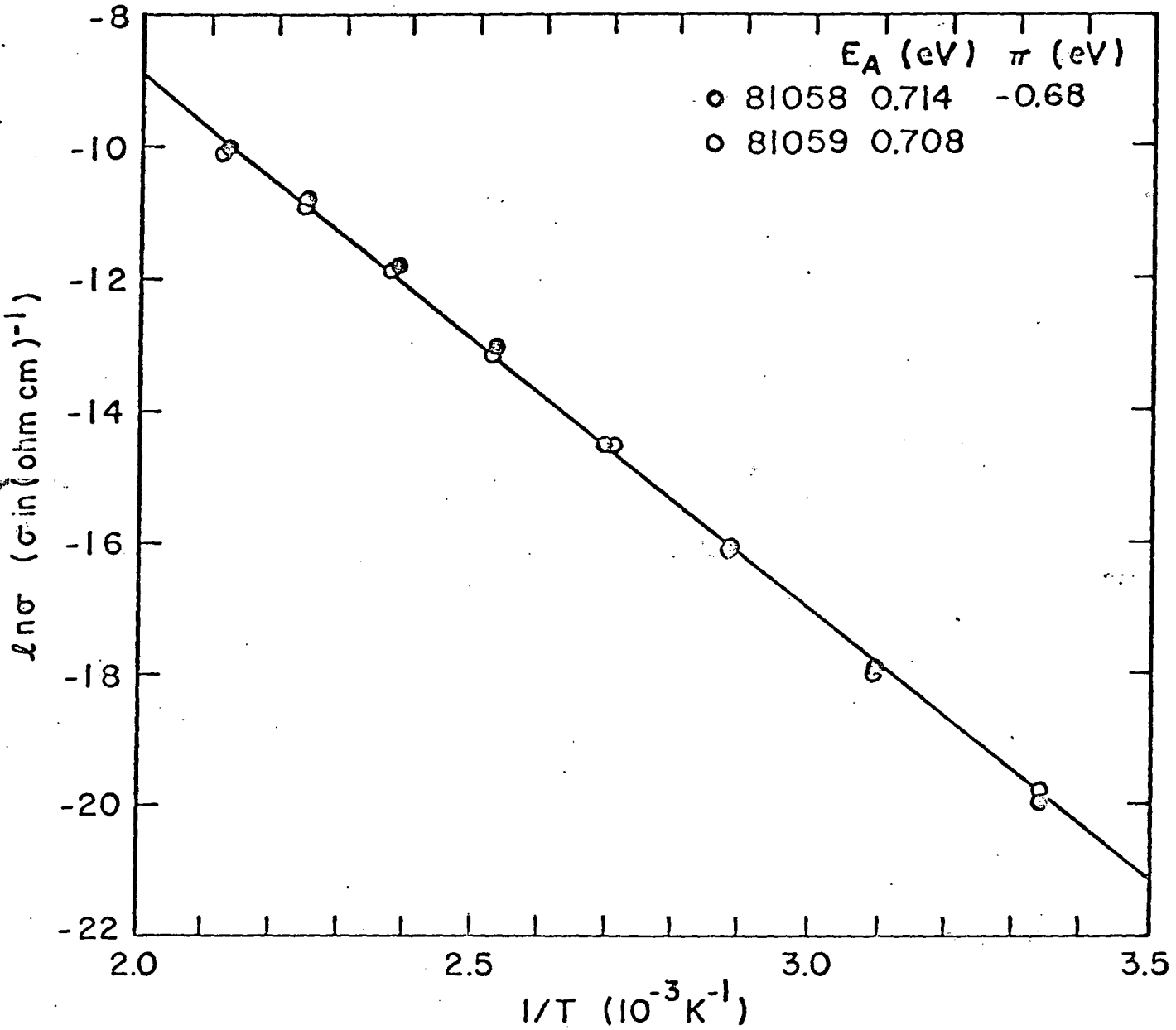

Figure 3

IEC81094

Activation Energy of two different

a-Si:H Films.

We do not understand these results, but we can postulate that the layers nearest the substrate may be very different from layers further away. In such a case, a coplanar measurement technique such as (T) may not reveal any significant differences, but a through-the-film measurement technique such as mobility measurement will reveal differences.

We also studied mobility as a function of growth rate. We see a distinct influence of growth rate, with the film with the faster growth rate having a larger μ_n. See Figure 4. Once again, we do not understand these results, except to speculate that a faster rate may lead to less contamination of the film from the walls of the reactor.

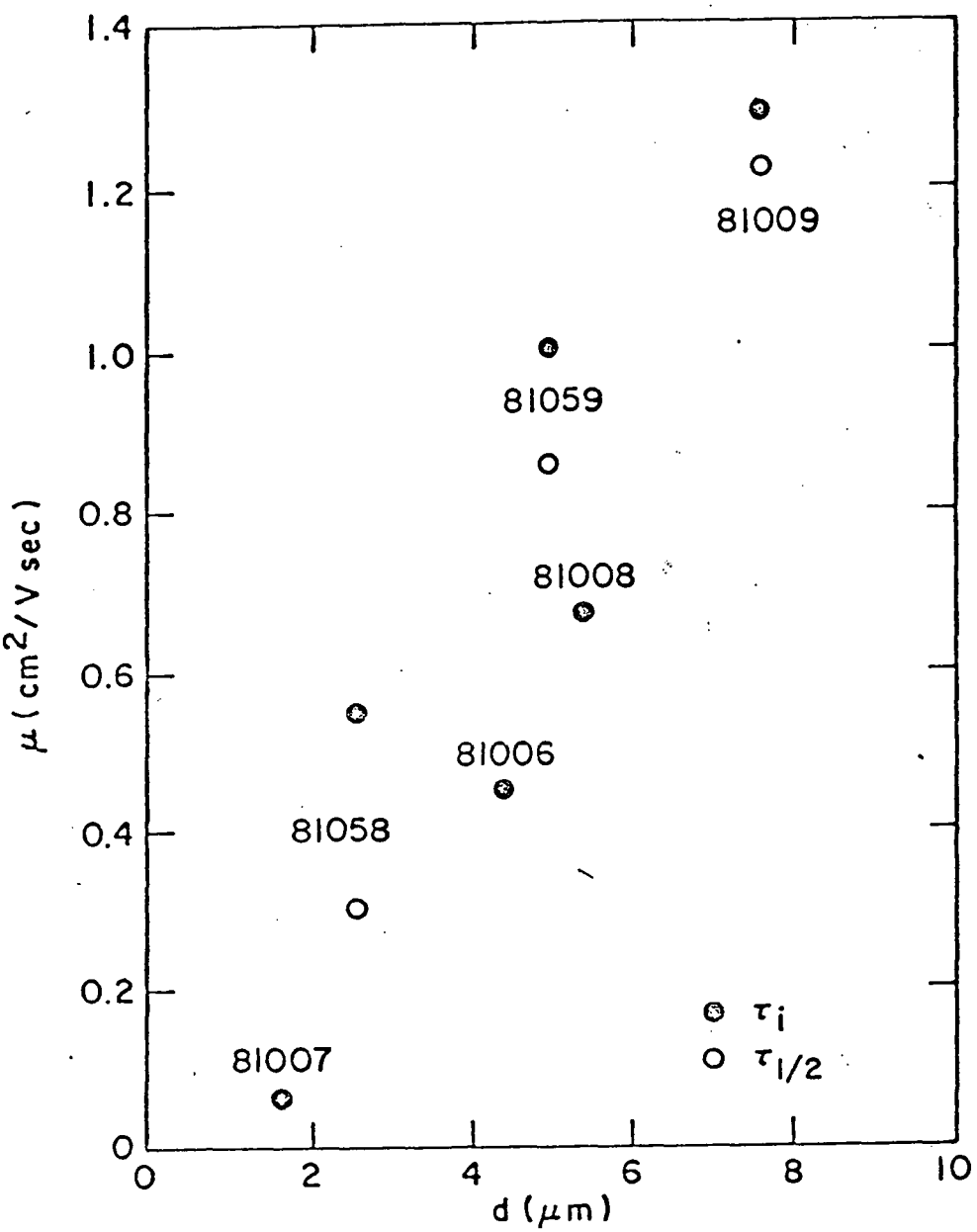

Figure 4. Mobility as a function of growth rate and thickness. Samples 81006-81009 were grown at 7 A/sec. Samples 81058-81059 were grown at 10.5 A/sec. τ_i indicates values computed from the point of inflection. $\tau_{\frac{1}{2}}$ from the half maximum point.

III. Device Fabrication and Analysis

1. Development of ITO Contact.

During this quarter, we have developed a technology for evaporating Indium-Tin Oxide (ITO) for use as a transparent contact to nip cells. We have used electron beam evaporation of (90% In_2O_3, 10% SnO_2) charge in an O_2 leak to achieve good transparency ITO contacts. The pressure in the bell jar during evaporation is maintained at 10^{-4} Torr, and the samples are heat treated in air for 5-60 minutes to achieve 95% transparent, $\sim 200\ \Omega/\square$ resistivity films.

In Figure 5, we show the influence of annealing time on the resistance and absorption of ITO films. In Figure 6, we show the typical absorption of curve for ITO films. It is apparent from Figure 5 that a temperature of $> 220^{o}C$ is needed so as to achieve low resistance and low absorption.

2. Analysis of Quantum Efficiency of a-Si nip Solar Cells.

The results reported during the previous quarter on QE of a-Si cells have been analyzed using an analytical model which can be used to estimate ($\mu\tau$) product of minority carriers. The analysis shows that electrons (and not holes) are the minority carriers in our cells. The analysis has been used to obtain $\mu\tau/_n \approx 1\text{-}2 \times 10^{-9}$ $cm^2/V\text{-}sec$. The details of the analysis are in Appendix B.

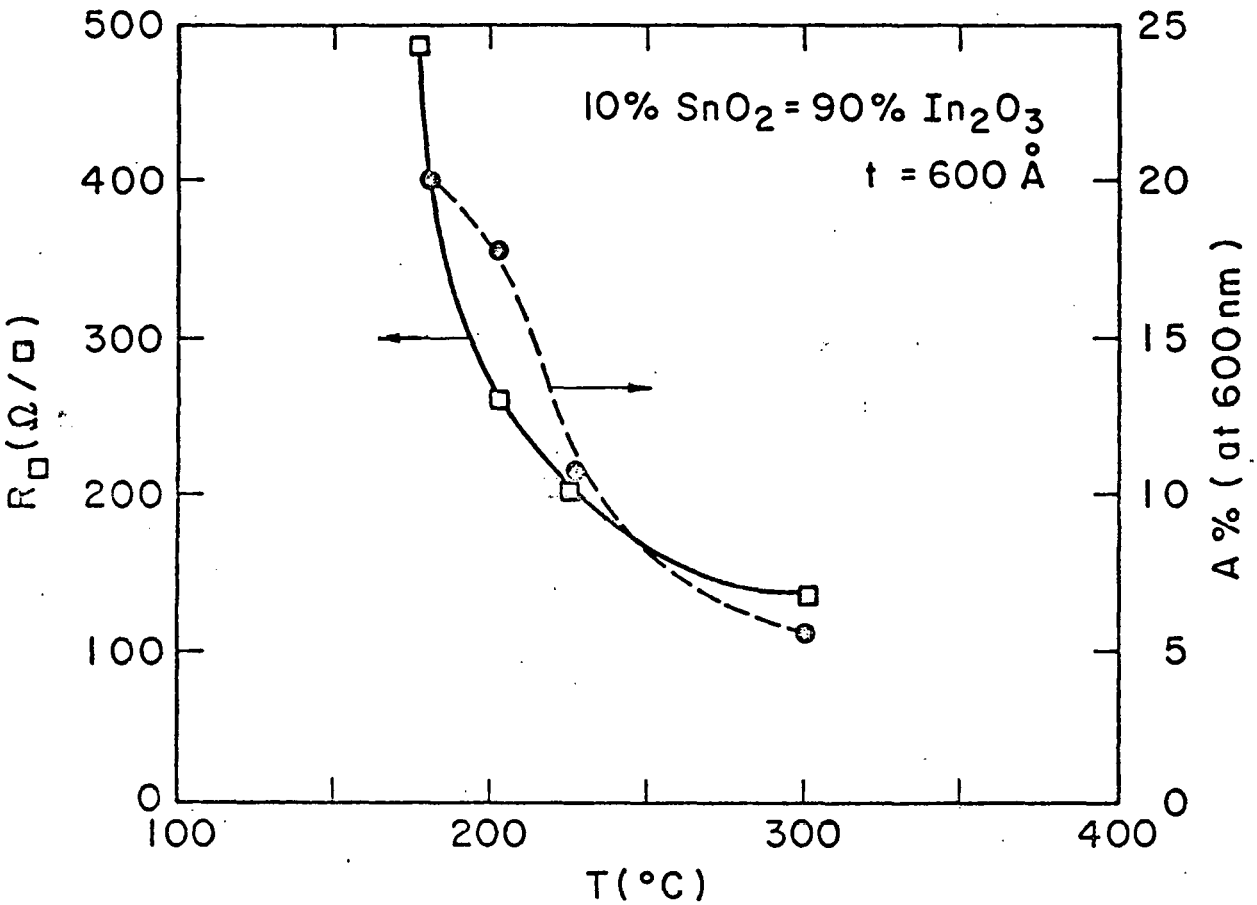

Figure 5. Resistance and Absorption of Evaporated ITO Films.

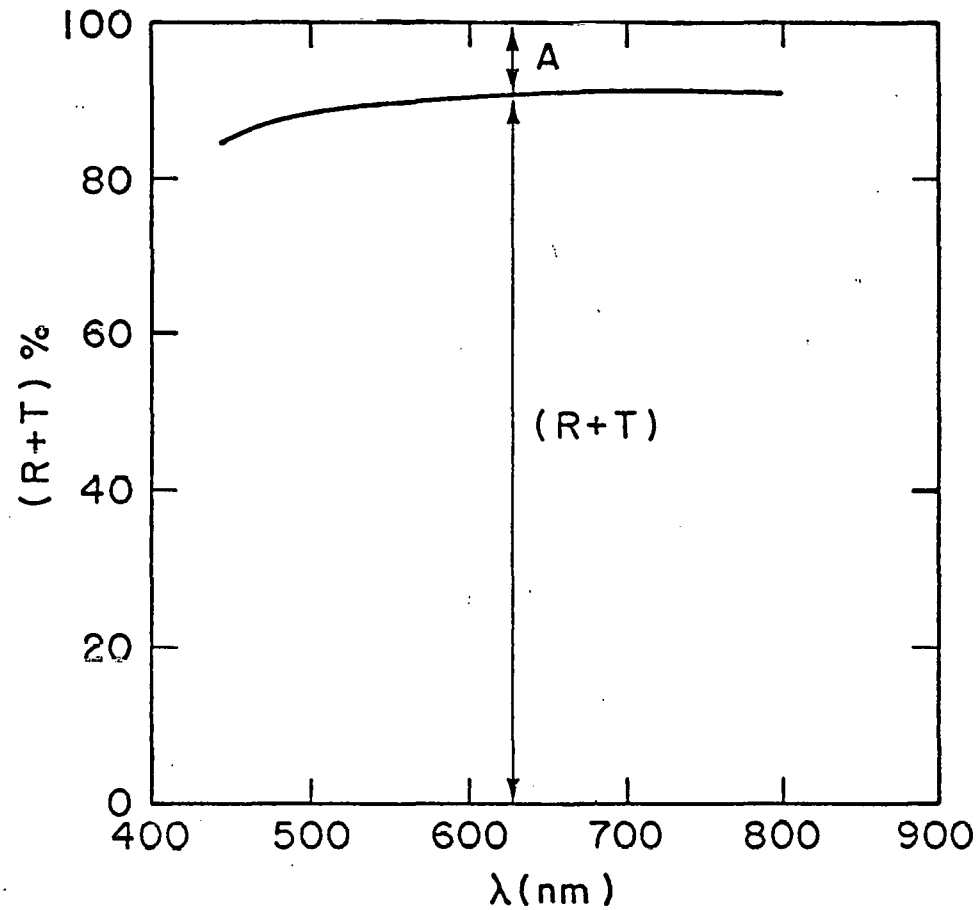

Figure 6. Absorption of ITO Film Annealed at 220°C.

IV. Advanced Device Design

It has been known for some time now that increasing the current output of an nip a-Si solar cell will depend upon increasing the optical path in i layer without decreasing the electric field. During this quarter, we have designed a new type of a-Si cell structure which can achieve this desired increase in optical path without sacrificing the electric field. The structure is a "Multiple-gap, parallel-connected, tandem cell".

The design of the structure is shown in Figure 7. It consists of two back-to-back a-Si cells connected by a transparent ITO layer. Thus, the structure may be a nip/ITO/pin cell.

The following advantages of our novel cell are immediately apparent.

i) Each cell has a nip configuration, thus allowing for two field regions in each cell.

ii) The i layer in each cell can be thin (~ 0.5 μm), thus allowing for efficient current collection and minimum fill factor loss.

iii) The transparent conductor (ITO) allows for complete photon transmission into the second cell.

iv) The low series resistance of ITO (~ 10 $\Omega/\square$) allows a wide cell-strip to be made (~ 1 cm).

v) Since the cells are electrically in parallel, changes in solar spectrum or accidental changes in cell thickness due to slight variations in processing have little influence on cell characteristics, in contrast to tandem, series-connected cells.(7,8)

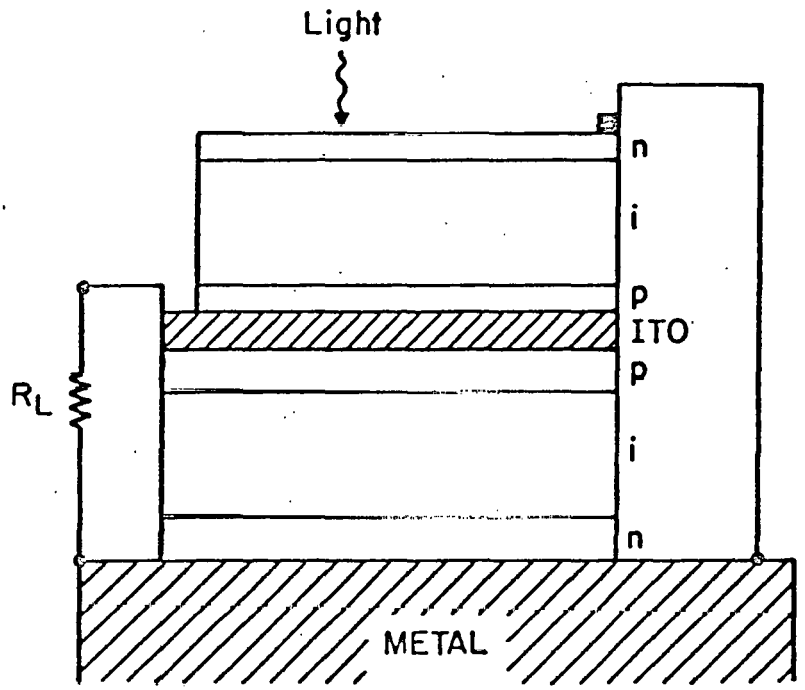

Figure 7. Schematic cross-section of a tandem-parallel configuration of amorphous thin-film solar cells.

One can calculate the anticipated performance improvement by using the absorption curve for a-Si and typical collection efficiencies. Using a typical a-Si absorption curve (Figure 8), increasing the absorption thickness from 0.5 to 1.0 μm leads to an increase in 2.4 mA/cm^2 in photon current under 100 mW/cm^2 illumination. At ~85% collection efficiency, this translates into ~ 2.1 mA/cm^2 current. Since the typical current for a 0.5 μm thick single-cell is 12 mA/cm^2, adding a second cell can lead to ~ 17% increase in current. Of course, if we put a good reflector behind the tandem cell, i.e. grow the cell on a highly reflecting substrate, we can further increase the absorption thickness to 2.0 μm, from 0.5 μm typical for a single cell on a poorly reflecting substrate (such as stainless steel). Then we can get ~25% increase in current, to about 15 mA/cm^2 external (or real) current. That would be a significant increase indeed.

Another interesting possibility is to use the two cells of different bandgaps, with the first cell having a bandgap larger than the second cell. In such a case, the cell outputs would be electrically isolated and we would have two solar cells circuits, each individually loaded. A simple way of doing this would be to use the connecting ITO layer as the ground contact. With differing bandgap isolated cells, we get the exciting possibility of better utilization of solar spectrum without the problems associated with bandgap and current matching inherent in multiple-gap series connected cells.(9)

It is hoped that both these designs can be used to improve efficiency of a-Si solar cells in the future.

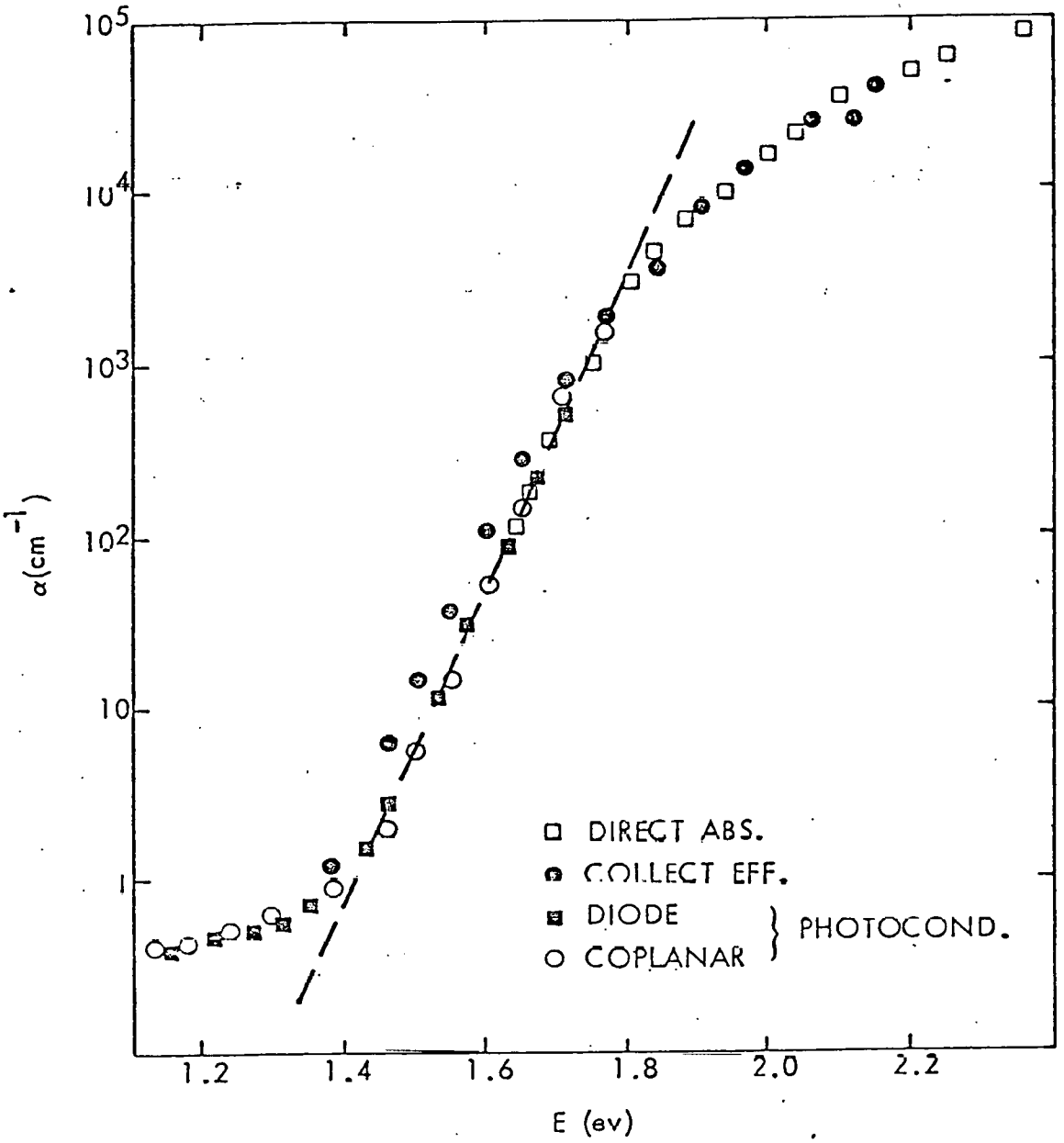

FIGURE 8

Absorption Coefficient of a-Si:H

(Source: B. Abeles et al., Solid-State Comm.,1980)

References

1. Y. Nagata, A. Kunioka and S. Yamazaki, Appl. Phys. Lett. 38, 142 (1981).

2. A. Matsuda et. al., "Tetrahedrally Bonded Amorphous Semiconductors", AIP Conf. Proc., Vol. 73, 192 (1981).

3. We are grateful to Dr. David Carlson of RCA for suggesting that DC (cathodic) films may be easy to microcrystallize, leading to high conductivity.

4. G. Dohler, Phys. Rev. B19, 2083 (1979).

5. V. L. Dalal et. al., 4th Quarter Progress Report, on SERI-XG-0-9195 (1981).

6. P. H. Nielsen and V. L. Dalal, Appl. Phys. Lett. 37, 1090 (1980).

7. Y. Hamakawa, H. Okamoto and Y. Nitta, Appl. Phys. Lett. 35, 187 (1979).

8. J. Hanak, J. Noncryst. Solids 35-36, 755 (1980).

9. V. L. Dalal and E. A. Fagen, Proc. 14th IEEE Photovoltaic Conf. (San Diego, CA, 1980). p. 1066

ANALYSIS OF CONDUCTIVITY AND THERMOELECTRIC POWER MEASUREMENTS ON AMORPHOUS SEMICONDUCTORS

Paul Nielsen
University of Delaware, Institute of Energy Conversion
Newark, DE 19711

ABSTRACT

Döhler's method of analyzing the results of conductivity and thermopower of amorphous semiconductors is examined by applying it to $\sigma(T)$ and $S(T)$ calculated exactly from several models of the density of states $N(E)$ and mobility $\mu(E)$. The method works well in determining the Fermi level shift with temperature, but provides limited accuracy in reproducing the conductivity $\sigma(E)$. The reliability of the alternative two channel model for $\sigma(T)$ and $S(T)$ is examined by computerized least squares fitting of the seven parameters to data of Jones, et al. I find quite different parameter sets reproduce the data equally well.

METHODS

The conductivity $\sigma(T)$ and thermopower $S(T)$ in amorphous semiconductors can be described by the following expressions:[1,2,3]

$$\sigma(T;n) = e\int_{-\infty}^{\infty} N(E)\mu(E,T)F(T;n)(1-F(T;n))dE \quad (1)$$

$$S(T;n) = k\int_{-\infty}^{\infty} N(E)\mu(E,T)((E-E_F)/kT)F(T;n)(1-F(T;n))dE/\sigma(T;n) \quad (2)$$

where $F(T;n)$ is the Fermi function for doping level n and E_F is the Fermi energy at temperature T.

If conduction occurs in extended states above E_c, and in localized states at energy E_L with a hopping activation energy W, the two channel model[1,4] gives $\sigma=\sigma_c+\sigma_L$ and $S=(S_c\sigma_c+S_L\sigma_L)/\sigma$ where:

$$\sigma_c = \sigma_{oc}\exp(-(E_c-E_F)_o/kT) \quad (3)$$

$$\sigma_L = \sigma_{oL}\exp(-(E_L-E_F+W)_o/kT) \quad (4)$$

$$S_c = -(k/e)(E_c-E_F)_o/kT+S_{oc} \quad (5)$$

$$S_L = -(k/e)(F_L-E_F)_o/kT+S_{oL} \quad (6)$$

To analyze experimental data requires the determination of the seven parameters defined above by a curve fitting procedure.

Döhler[5] has introduced a method of analyzing conductivity and thermoelectric power measurements which simultaneously uses both $\sigma(T)$ and $S(T)$ data to obtain values of the Fermi level shift with temperature and the differential conductivity $\sigma(E)$. The method is also useful in examining whether doping induced shifts of the Fermi level also produce changes in the conductivity $\sigma(E)$. Because the Fermi function is approximated by the Maxwell-Boltzman distribution and the statistical factor for the final state of the scattering process is set equal

to 1, the approach is not applicable to situations in which the Fermi level lies within a region of high conductivity.[6]

The method relies upon specific relationship between functions V(T) and W(T) and the experimental values of σ(T) and Peltier energy π(T) = eS(T)T, for various levels of doping n_D:

$$\sigma(T;n_D) = \sigma_o(T)\exp\{[E_o-E_F(T;n_D)]/kT\} \quad (7)$$

$$\sigma_o(T) = \sigma_{oo}\exp\,[-V(T)/kT] \quad (8)$$

$$-\pi(T) = W(T)+E_o-E_F(T;n_D) \quad (9)$$

where E_o is an arbitrary reference energy which should be independent of doping.

Equations (7), (8), (9) may be combined as

$$\ln\sigma(T)-eS(T)/k = \ln\sigma_{oo} +[W(T)-V(T)]/kT \quad (10)$$

Because V(T) and W(T) are defined to be doping independent, the quantity $\ln(\sigma(T)/\sigma_{oo})-eS(T)/k$ is independent of doping and hence independent of $E_F(0;n_D)$ if μ(E) and N(E) do not change with doping level. A simple Laplace transform allows one to obtain σ(E) = eN(E)μ(E), if $W(T)-V(T) = nk(T-T_o)$.

In order to evaluate the reliability and accuracy of Döhler's method of analysis it is necessary to have a set of σ(T;nD) and S(T;nD0 values applicable to known density of states N(E), mobility μ, and $E_F(0)$ values. Such values were obtained for a number of N(E) and μ(E) functions by accurate numerical integration of equations (1) and (2) as described in Ref. 6.

RESULTS AND DISCUSSION

Jones, et al.[4] have presented an analysis by the two channel model of a number of phosphorous doped amorphous silicon samples. Their experimental results are quite similar to the ones analyzed with success by Döhler[5] using a distributed conductivity. In order to evaluate the uniqueness of the parameters presented in (4), the S and σ points of their sample 8 were digitized and entered into a computer program which calculates the RMS deviations of S and of $\log_{10}\sigma$ from the calculated points at the same values of T.

Table I. Selected parameter sets, and RMS deviations for Sample 8 of Ref. 4. S_o values in mV/K, and RMS ΔS in μV/K, other energies in eV.

Set	σ_{oc}	E_c-E_F	σ_{oL}	E_L-E_F	W	S_{oc}	S_{oL}	RMS logσ	RMS ΔS
Jones	24	0.24	3	0.08	0.12	-0.56	-0.56	0.0178	26.17
1	23.2	0.24	3	0.08	0.12	-0.56	-0.56	0.0159	24.17
2	23.2	0.24	3	0.04	0.16	-0.5	-0.80	0.0159	24.40
3	23.2	0.24	3	0.00	0.20	-0.43	-1.035	0.0159	24.05

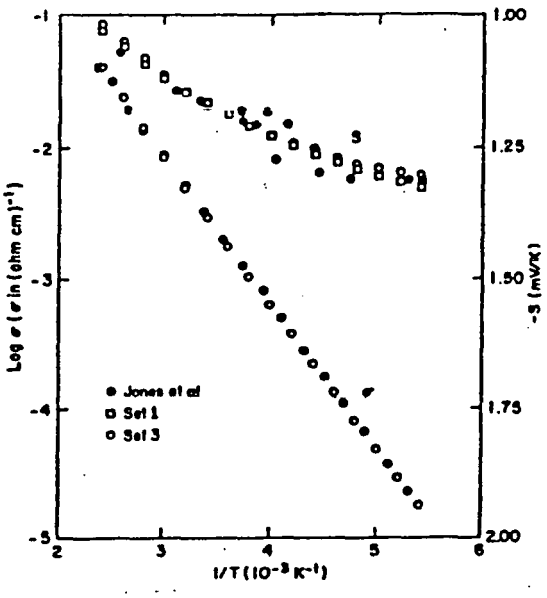

Fig. 1 S(T) and σ(T) and the two channel fits to the data.

It is evident from Table I that the choice of parameters made by Jones, et al is reasonably good. But by relaxing their essentially arbitrary requirements that $S_{OC} = S_{OL}$ it is possible to vary $E_L - E_F$ from 0.08 to 0, while at the same time increasing W from 0.12 to 0.20, and changing S_{OC} and S_{OL}, to maintain or slightly improve the fit to the S data. Fig. 1 shows that the calculated values of S(T) for parameter sets 1 and 3 differ only slightly from each other. From this example I conclude that one cannot expect to get a unique set of two channel parameters if one allows $S_{OC} \neq S_{OL}$, as is physically reasonable.

Let us now consider the results of a Döhler analysis of calculated S(T) and σ(T) points. Two examples will be considered here. In both of them N(E) varies from 10^{17} to 10^{22} states eV^{-1} cm^{-3} according to:

$$\log N(E) = 17(g-h)+22(h-g+1) \qquad (11)$$

with $g = [1+\exp(E/W)]^{-1}$, $h = [1+\exp[(E+Eg)/W]]^{-1}$, W = 0.15, and Eg = 1.4eV. However an additional peak centered at -0.2eV, with height of 0.699 in log N(E) and Lorentzian half width 0.05 is included in the second example. This peak has negligible effect on the results. μ(E) is given by:

$$[1+\exp\ [|40(0.2-E)|^{x}\mathrm{sign}(0.2-E)]]^{-1} \qquad (12)$$

where x is 1.4 for the second case (CS211) and 20 for the first case (CS209). Thus the second case has a gradual fall off in σ(E), as shown in Fig. 5, while the first case has a rapid decrease to zero, also shown in Fig. 5, and thus represents more closely the case of a crystalline semiconductor. Figs. 2 and 3 give the calculated σ(T) and S(T) for the second case. Also shown on the Figs. are the input values of $E_F(0)$, activation energies in eV for different parts of the curves, and the values of A ($=eS_o/k$ in Eqs. (5) or (6)). The results for the first case are generally similar to the higher T portion of these figures, with the activation energies remaining almost constant as the temperature is decreased.

The Döhler analysis for both cases are shown in Fig. 4, with the upper set of curves (for CS209) displaced vertically 100meV for clarity. In both cases the curves for W, V, and W-V for the different $E_F(0)$ values from -0.5 to 0.0 lie atop one another, as Döhler predicted for an unchanging conduction mechanism. The variation of E_F with T cal-

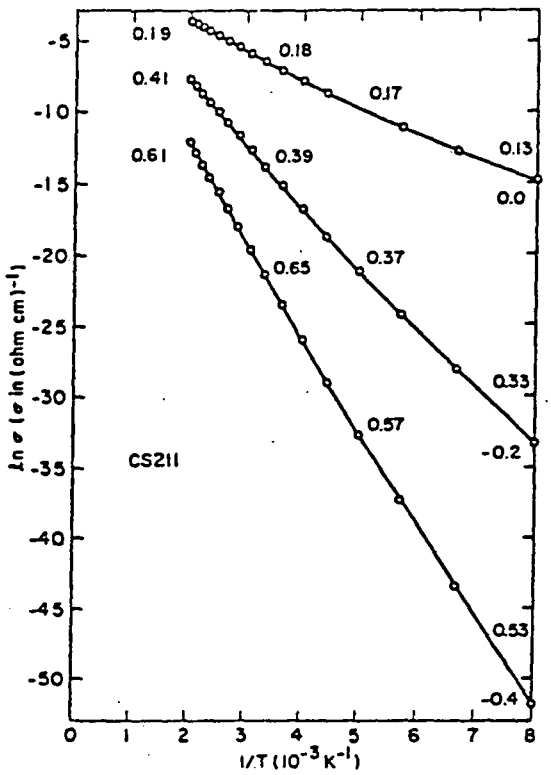

Fig. 2 $\sigma(T, E_F(0))$ for CS211

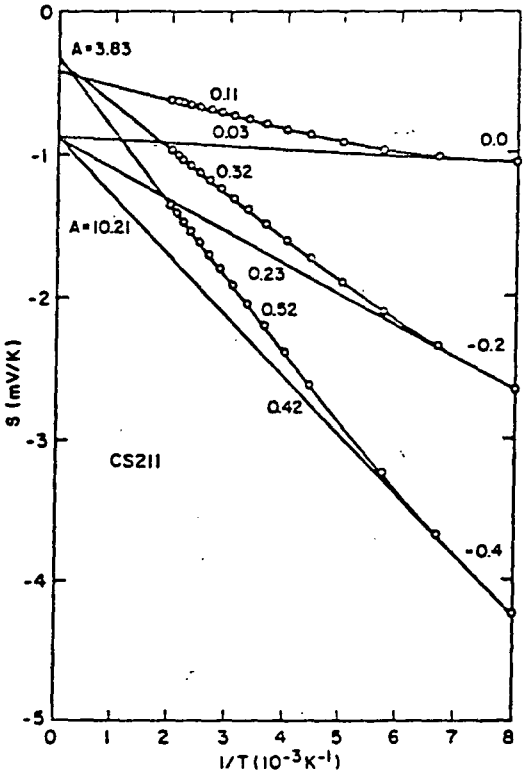

Fig. 3 $S(T, E_F(0))$ for CS211

culated from the Döhler analysis is within 10% of the variation calculated during the generation of $\sigma(T)$ and $S(T)$.

In order to apply the simple Laplace transform given by Döhler in his Eq. 28 (in which the cosine factor should be $\cos[x(\tilde{\epsilon} + n\ln x - \pi)]$), W-V must be linear in T. This is the case for Model. CS211. Model CS209 gives a slightly curved W-V. The deviations from linearity is, however, relatively small and it is not clear that one would necessarily decide that W-V was curved if the points also suffered from experimental noise.

The insignificant deviations of W-V of CS211 from linearity produces deviations of $\sigma_T(E)$ from $\sigma(E)$ of less than a factor of 3 at worst, and mostly less than 25%. However, the small deviation of W-V from linearity in Model CS209 results in a factor of 10 error above the mobility edge, and a very large error below it.

I conclude that this method gives good results for the Fermi level shift with temperature and a reasonable indication that the transport mechanism is not changing with Fermi level. But it will not determine $\sigma(E)$ to better than a factor of 3-10 if there is any sharp structure in $\sigma(E)$, such as a sharp mobility edge, or narrow peaks in N(E) near the mobility edge.

ACKNOWLEDGMENTS

This work was supported by Contract # SERI-XG-0-9195-1.

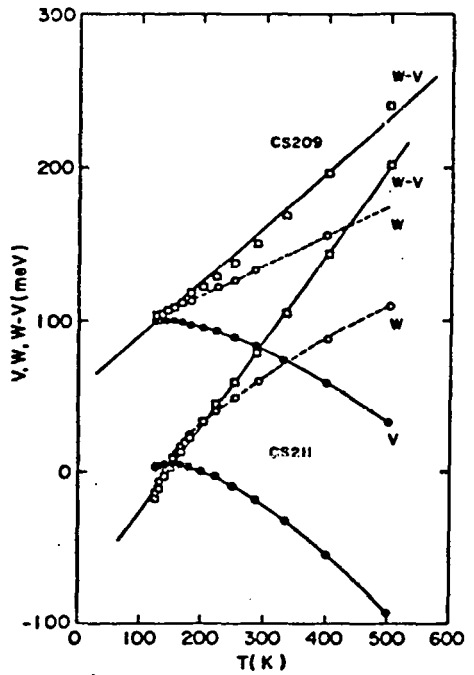

Fig. 4 Döhler analysis

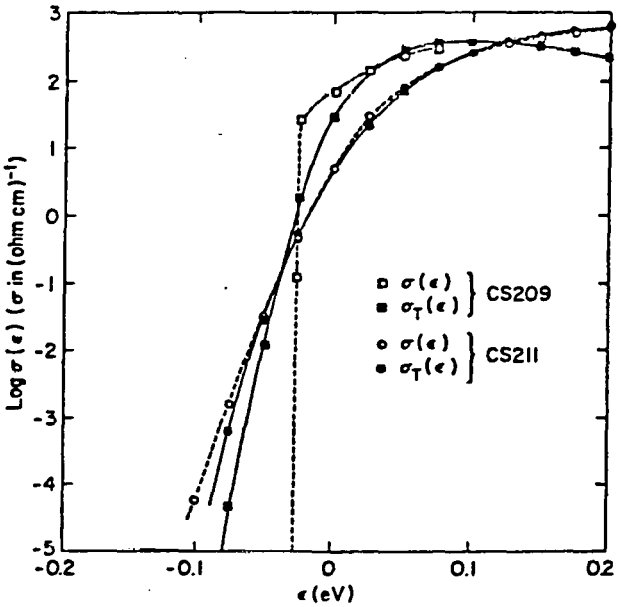

Fig. 5 Input σ(E) and Laplace result $\sigma_T(E)$

REFERENCES

1. N. F. Mott and E. A. Davis, Electronics Processes in Non-Crystalline Materials, 2nd Ed. (Oxford U. Press, Oxford, 1979) Chapters 2 and 7.

2. M. Cutler and N. F. Mott, Phys. Rev. 181, 1336 (1969).

3. H. Fritzsche, Solid State Commun. 9, 1813 (1971).

4. D. I. Jones, P. G. LeComber and W. E. Spear, Phil. Mag. 36, 541-551 (1977).

5. G. H. Döhler, Phys. Rev. B 19, 2083-2091 (1979).

6. P. Nielsen and V. L. Dalal, Appl. Phys. Lett. 37, 1090-1092 (1980).

(To be published in Proceedings of 9th. International Conference on Amorphous and Liquid Semiconductors, Grenoble, France, 1981)

"Minority Carrier Transport in Depletion Layers of nip a-Si:H Solar Cells"

Vikram Dalal and Fernando Alvarez

Institute of Energy Conversion
University of Delaware
Newark, Delaware 19711

Abstract

Transport properties of electrons and holes in i layers of pin a-Si solar cells are important in determining the current collection efficiency of these cells. In this paper, we describe a new technique for measuring the ($\mu\tau$) product of minority carriers in the undoped layer of an a-Si:H cell. It is shown that the transport properties in depletion layers of solar cells can be very different from the transport in virgin i layers, and that under certain circumstances, electrons can become the minority carriers, in strong contrast to virgin i layers, where holes are the minority carriers.

Introduction

The current collection efficiency of a-Si:H solar cells is limited by the transport properties, particularly ($\mu\tau$) products and diffusion lengths L_n and L_p of electrons and holes. Generally speaking, it is assumed that the ($\mu\tau$) product of holes is much smaller than that of electrons (1-3), and hence, holes are the limiting or minority carriers (4,5). However, no reliable evidence exists that such is indeed the case in the i layer of a pin cell. In this paper, we discuss a new technique for identifying the limiting carrier and for estimating its ($\mu\tau$) product in pin cells. We shall show that under certain circumstances, the electrons may have a lower ($\mu\tau$) product than holes and may serve as minority carriers. It is postulated that such a condition can arise because of cross-contamination between the p^+ and i layers during the growth of the cell.

Basic Model

The basic model for analyzing the current collection efficiency of pin cells is shown in Figure 1 (5). The model states that there are <u>two</u> junctions in a n^+ip^+ a-Si:H solar cells, the front n^+i junction and the back ip^+ junction. Thus, there are two depletion regions, separated by a neutral region of low field. The spatial extent of the field regions depends upon the density of states (5). If the density of states in the mid-gap region is high, the depletion thicknesses t_1 and t_2 are small, and neutral region thickness t_2 is large. If the mid-gap density is low, the depletion thicknesses overlap and there is no neutral region.

In this case, the potential in the i layer can be approximated by a Mott barrier (6), but with sharp potential profiles at the edges.

Using the basic model of Figure 1, we can predict the behavior of the collection efficiency of a-Si solar cells with applied voltage. As the applied voltage in the forward direction increases, the depletion regions will shrink, and the neutral region will increase. Consequently, if the diffusion length of carriers is small, the carrier collection efficiency will decline. Conversely, for reverse applied voltage, the collection efficiency will increase. Similar considerations hold for the Mott-barrier case, where a forward voltage reduces the field, and a reverse voltage increases the field. Since the carriers rely on field assisted transport, if the range of carriers ($\mu\tau E$) is comparable to the film thickness, the carrier collection efficiency will increase with reverse voltage and decrease with forward voltage. Therefore, a measurement of collection efficiency with bias voltage provides a tool for measuring ($\mu\tau$) products.

Analysis

Electric Field Profile: The electric field and potential profiles in the i layer depend upon the density of states in the mid-gap (7). Recent results on the measurement of density of states in a-Si:H by DLTS (8,9) and by mobility transport (10) show that the density of states in a-Si:H is well represented by Figure 2, with sharp tails near the band edges and a flat density $\sim 10^{16}/cm^3$-eV in the middle. In such a case, for a thin i layer ($\sim$ 0.4 μm), the electric field extends over the entire i layer; i.e., a Mott barrier exists.

For simplicity, we can assume that the field is uniform, given by $E \approx (V_D + V)/t_i$, where V is applied voltage, V_D the diffusion voltage, and t_i the thickness of i layer. V_D is given by: $V_D = E_g - \Delta E_{f,n} - \Delta E_{f,b}$, where E_g is the bandgap, $\Delta E_{f,n} = (E_c - E_{f,n})$ on the n-side; $\Delta E_{f,p} = (E_V - E_{f,p})$ on the p-side. Typically, we measure $\Delta E_{f,n} = 0.25V$, $\Delta E_{f,p} = 0.4V$ and $E_g = 1.7V$. Thus, $V_D = 1.05V$ and $E \lesssim 2.5 \times 10^4 V/cm$ in our sample at zero bias.

For simplicity, we can also assume that only one kind of carrier is important; i.e., $(\mu\tau)$ product for one carrier << that of the other. Then, the following equation holds for quantum efficiency $QE(\lambda)$, of photogenerated carriers, assuming a nip/metal cell (light incident from n side) and electrons the minority carriers in the i layer.

$$QE(\lambda) = \frac{\alpha S_n}{1 + \alpha S_n} \left[1 - \exp\left(-\frac{t}{S_n}(1 + \alpha S_n)\right)\right] \qquad (1)$$

where α is the absorption coefficient and $S_n = (\mu\tau)_n \cdot E$ is the range of electrons. Therefore, from the dependence of $QE(\lambda)$ on V, we should be able to obtain $(\mu\tau)_n$.

Experiment

The experiment consisted of measuring the quantum efficiency $QE(\lambda)$ of nip/metal a-Si solar cells. A typical cell was made by depositing successively p, i and n layers on a Ti/7059 substrate. The thickness of n layer was 200Å and i layer, 4200Å. A semi-transparent 75Å thick Ti dot of $0.20cm^2$ active area was deposited on the n layer and monochromatic light was incident on the Ti dot. The absorption of the Ti dot was measured at ~ 10% and the reflection

from the Ti/a-Si combination was ~45%, allowing ~ 45% light transmission. The monochromatic beam was chopped and QE(λ) measured as a function of voltage in the presence of a white-light bias at AM1 illumination level so as to approximate the conditions faced by the solar cell in actual operation (11).

In Figure 3 we show the internal QE(λ) of the cell under three voltage conditions, zero bias and $\pm$ 0.4V. It is immediately obvious that the range of carriers is comparable to thickness, so that a reduction in field causes a reduction in QE. Much more information can be obtained by plotting the ratio QE(V)/QE(V = 0) vs. wavelength, which is done in Figure 4. A striking feature of Figure 4 is that the carriers generated deeper in the i layer (long λ photons) suffer much greater reduction in QE than carriers generated nearer the n^+ layer (short λ photons). This can be true only if the minority carrier is of the type which has to traverse towards the n^+ layer to be collected; i.e., if the minority carrier is an electron. Thus, the shape of QE(V)/QE(V = 0) curve gives us the <u>type</u> of carrier with the smaller $\mu\tau$ product.

Quantitative information is obtained by measuring QE(λ) vs. voltage for several wavelengths, and then fitting to Equation 1 to determine S_n, knowing α. This is done in Figure 5, where we plot analytical curves from Equation 1 for three wavelengths, 0.5, 0.6, and 0.7 μm. The relation between QE(λ) and S_n is computed from the experimental QE(λ) vs. voltage data using an iterative process with ($\mu\tau$) as a fitting parameter. The fit between the analytical expression and the data points (+ + +) is seen in Figure 5. We obtain an estimate of $S_n \approx 0.25$ μm at V = 0, giving ($\mu\tau$) for electrons $\approx 10^{-9} cm^2/V$. Note that the fit between experimental and analytical curves deteriorates at extreme voltages because the model is no longer valid at those voltages. This value of ($\mu\tau$) can now be used to fit Figure 4 (solid lines) and it is seen that the fit is quite good. Thus, our

simple model fits the experimental QE curves quite well. Due to the simplicity of the model, the value of $(\mu\tau)$ is accurate only to approximately $\pm$ 25%.

Conclusion

In conclusion, we have described a new technique for determining the $(\mu\tau)$ product of minority carriers in i layers of nip a-Si:H solar cells. A surprising conclusion is that the electrons are the minority carriers, a probable consequence of the severe p-type contamination that exists in i layers made immediately after depositing the p-layer. Clearly, for making high quality cells, this cross-contamination problem will have to be addressed and solved.

This work was partially supported by Solar Energy Research Institute under subcontract XG-9-9195.

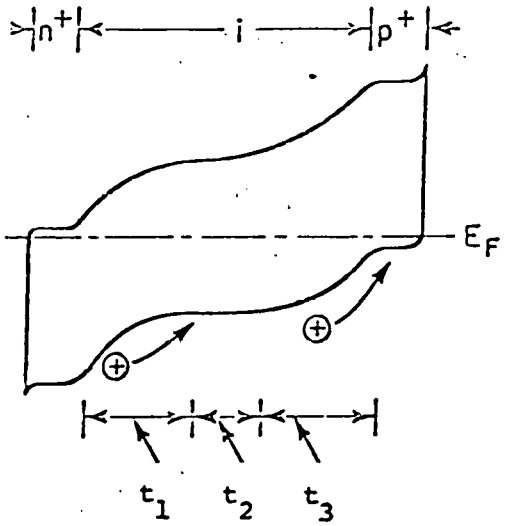

Fig. 1

Band Diagram for a-Si:H nip junction

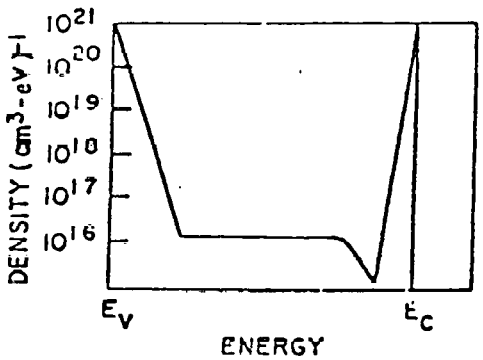

Fig.2

Approximate Density of States
in a-Si:H

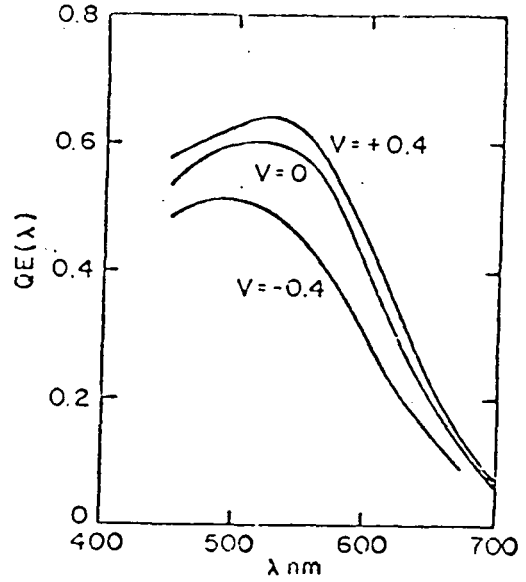

Figure 3

Quantum Efficiency of nip cell for short-circuit, forward (-) and reverse (+) voltage.

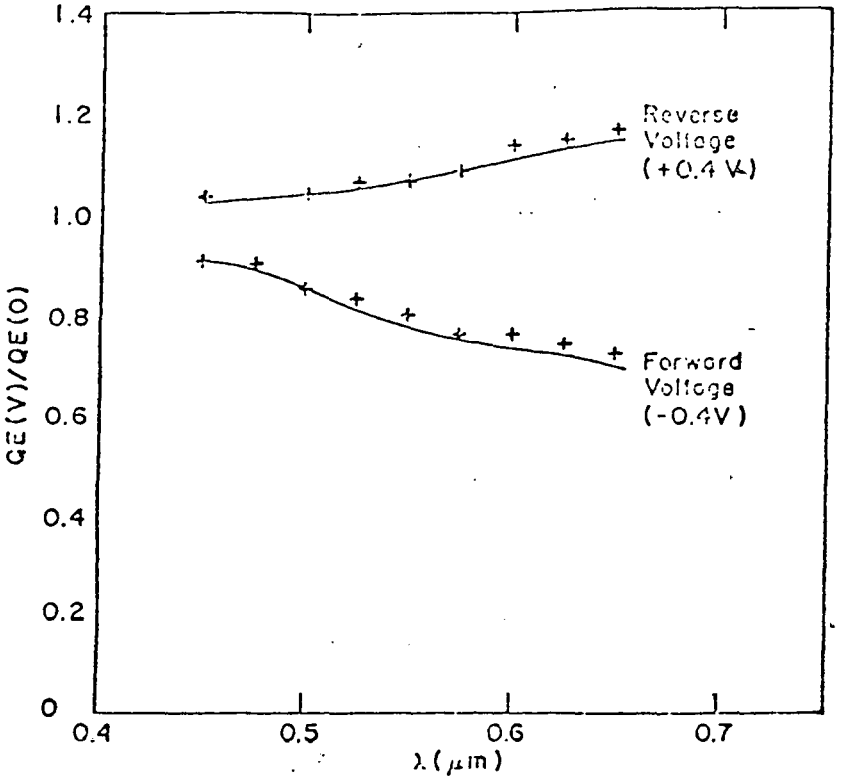

Figure 4

Ratio of Quantum Efficiencies vs. wavelength.

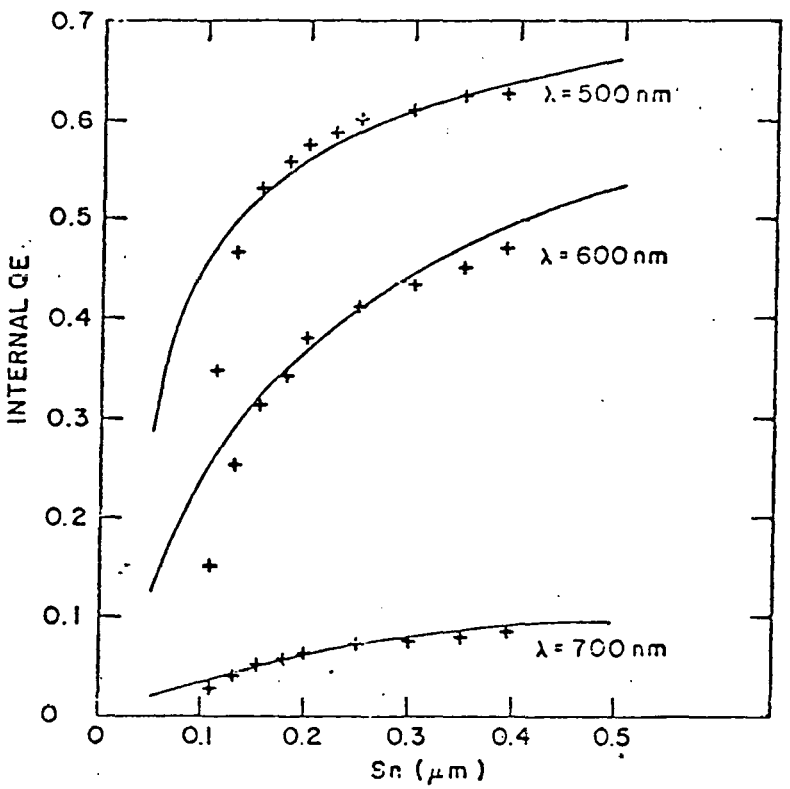

Figure 5

Experimental and analytical curves of QE vs. Range S_n

References

1. Debney, B. Solid-State Electron Devices 2 - Special Issue; (1978) 515.
2. Staebler, D. J. Noncryst. Solids, 35-36, (1980) 387.
3. Wronski, C. IEEE Trans. Electron Devices 24, (1977) 351.
4. Crandall, R., Williams R., and Tompkins, B. E. J. Appl. Phys. 50, (1970) 5506.
5. Dalal, V. L. Solar Cells 2, (1980) 261.
6. Bell, R. Appl. Phys. Lett. 36, (1980) 936.
7. Spear, W., Le Comber, P., and Snell, A. J. Phil. Mag. B38, (1978) 303.
8. Cohen, J. D., Lang, D., and Harbison, J. P. Phys. Rev. Lett. 45 (1980) 197.
9. Johnson, N. To be published in Proc. AIP Conf. on Tetrahedral Amorphous Semiconductors. (Carefree, Arizona, 1981).
10. Tiedje, T., and Rose, A. ibid.
11. Dalal, V. L., and Rothwarf, A. J. Appl. Phys. 40, (1979) 2980.

886498 PREV SN - 886497 R HDRB RM020582 RM020982 FILE-RM0205.E01

010 8202029821 030 Uncl 040 Y

070 Dalal, V.

110 Improved amorphous Si solar cells. Quarterly progress report No. 5, February 1-April 30, 1981

150 SERI/PR--9195-1-T3

240 Contract AC02-77CH00178

290 DE82006886

370 Nov 1981 390 37 430 NTIS, PC A03/MF A01

510 MN-63 520 p 530 EDB;ERA;NTS

540 EDB-140501;

550 TIC 580 United States of America (USA) 570 United States of America (USA)

700 950 6687;950 1261 710 Solar Energy Research Inst., Golden, CO (USA); Delaware Univ., Newark (USA). Inst. of Energy Conversion

AUG 820 - NONE

801 SILICON:T1;AMORPHOUS STATE;HYDROGEN ADDITIONS;SILICON SOLAR CELLS:T2;CRYSTAL GROWTH:Q1;ELECTRIC CONDUCTIVITY; SPUTTERING;N-TYPE CONDUCTORS;P-TYPE CONDUCTORS;CRYSTAL DOPING;CARRIER MOBILITY;THICKNESS;QUANTUM EFFICIENCY; ELECTRIC POTENTIAL;CARRIER LIFETIME;CHARGE CARRIERS:Q2;DESIGN;ELECTRIC CURRENTS;ELECTRIC CONTACTS;THERMOELECTRIC PROPERTIES;ELECTRICAL PROPERTIES:Q1,Q2;VACUUM EVAPORATION;

T;Q1 SILICON;CRYSTAL GROWTH

T;Q1 SILICON;ELECTRICAL PROPERTIES

T;Q2 SILICON SOLAR CELLS;CHARGE CARRIERS

T;Q2 SILICON SOLAR CELLS;ELECTRICAL PROPERTIES

950 Both n and p-type a-Si:H films with very high conductivities have been grown by diluting SiH_4 in Ar or H_2. These films have Fermi levels close to the conduction and valence bands (0.03 eV). The use of these heavily doped films as p^+ and n^+ junction layers in a p^+in^+ cell should increase the diffusion voltage of the diode, thereby increasing both J/sub sc/ and V/sub oc/. The analysis of conductivity and thermoelectric power on films of diverse thickness have revealed no systematic changes. However, the drift mobility shows a systematic increase with thickness. The analysis of cells by studying quantum efficiency vs. applied voltage has revealed the electron (μ tau) product is limiting transport in nip cells and not the hole (μ tau) product. Analysis reveals that typically (μ tau)/sub eta/ = 10^{-9} cm^2/V. A new device design, Tandem parallel-connected cells, has been evolved to improve the current collection in a-Si cells. This design may help increase J/sub sc/ to 15 to 16 mA/cm^2 in a-Si:H.

EDB ☒	INS ☐	TTR ☐	CATEGORIES
ERA ☒	RIP ☐	DOE ☒	1. 140501
EPA ☐	GAP ☐	☐	2.
WDA ☐	CRF ☐	☐	3.
			4.
			5.

AUGMENTATION:

SPLIT	DESCRIPTORS	FLAGS
	Silicon	T1
	Amorphous state	
	Hydrogen additions	
	Silicon solar cells	T2
	Crystal growth	Q1
	Electric conductivity	
	Sputtering	
	N-type conductors	
	P-type conductors	
	~~Electrochemical coating~~	
	Crystal doping	
	Carrier mobility	
	Thickness	
	Quantum efficiency	
	Electric potential	
	Carrier lifetime	
	Charge carriers	Q2
	Design	~~Q2~~
	Electric currents	
	Electric contacts	
	Thermoelectric properties	
	Electrical properties	Q1, Q2
	Vacuum evaporation	

LEW

Summary

~~1. Material Growth~~

Both n and p-type a-Si:H films with very high conductivities ~~[$\sigma > 10$]~~ have been grown by diluting SiH_4 in Ar or H_2. These films have Fermi levels close to the conduction and valence bands ($\lesssim 0.03$ eV). The use of these heavily doped films as p^+ and n^+ junction layers in a p^+in^+ cell should increase the diffusion voltage of the diode, thereby increasing both J_{sc} and V_{oc}.

~~2. Material Analysis~~

The analysis of conductivity and thermoelectric power on films of diverse thickness have revealed no systematic changes. However, the drift mobility shows a systematic increase with thickness. ~~We do not yet understand these results.~~

~~3. Device Fabrication and Analysis~~

The analysis of cells by studying ~~QE~~ quantum efficiency vs. applied voltage has revealed the electron ($\mu\tau$) product is limiting transport in nip cells and not the hole ($\mu\tau$) product. Analysis reveals that typically $(\mu\tau)_n \gtrsim 10^{-9}$ cm^2/V.

~~4. Device Design~~

A new device design, Tandem parallel-connected cells, has been evolved to improve the current collection in a-Si cells. This design may help increase J_{sc} to 15-16 mA/cm^2 in a-Si:H.